



Article citation info:

Yue C, Zheng X, Wang C, Liu H, Chen H, Modeling and Identification Method of Bolt Loosening of Joint Surface under Axial Tension of Multistage Disk-Drum Rotor
Eksploracja i Niezawodność – Maintenance and Reliability 2023; 25(2)
<http://doi.org/10.17531/ein/165779>

Modeling and Identification Method of Bolt Loosening of Joint Surface under Axial Tension of Multistage Disk-Drum Rotor

Indexed by:



Cong Yue^a, Xiangmin Zheng^a, Chaoge Wang^a, Hao Liu^b, Hu Chen^c

^a Logistics Engineering College, Shanghai Maritime University, Shanghai, China

^b AECC Commercial Aircraft Engine Co. LTD, Shanghai, China

^c SPIC Beijing Gas Turbine Energy Technology Development Co.LTD, Beijing, China

Highlights

- Connection characteristics of bolt screwing in the multi-exciting environment.
- An equivalent stiffness model analyses the effect of stiffness loss of joint surface with bolt missing.
- This method considers the influence of bolts at different locations on the stiffness loss.
- Multi-period excitation vibration experiment.
- Correlation coefficient evaluates the identification effect of different measuring points.

Abstract

Individual bolt at key connection positions is prone to loose when the engine is cycle-operating under complex loads. A joint surface equivalent stiffness model is derived and developed based on the connection characteristics of bolt screwing in the multi-exciting environment of the high-pressure rotor. The model is used to analyse the effect of bolt missing at circumferential positions with the equivalent stiffness loss. Vibration experiments under both axial force and lateral impact were carried out to obtain the dynamic response feature of the multistage disk-drum simulated rotor with missing one bolt at different positions. The Spearman correlation coefficient was applied to evaluate the identification effect of different measuring points on the bolt loosening position. The study shows that the eigenfrequencies of experimental results have a consistent trend with the equivalent stiffness variation caused by single bolt missing model. This method also provides a theoretical basis for the detection of bolt deviation position with multi-exciting vibration detection.

Keywords

multistage drum rotor; bolt loosening; equivalent joint stiffness; structural health monitoring

This is an open access article under the CC BY license (<https://creativecommons.org/licenses/by/4.0/>)

1. Introduction

Because of the simple structure and reliable performance, bolt flange joints are widely used as connection structures in rotary machines, such as aero-engine and gas turbine. The performance of the bolt connection not only determines the manufacturing quality, but also directly affects the reliability and stability of the multistage disk-drum rotor of aero-engine. Mechanical transfer characteristic of the bolt flange connection structure can present multiple complexities under dynamic loadings, which makes it difficult to detect the change of bolt

fastening property. The joint surface assembly technology is still the bottleneck in industry. The accurate evaluation and prediction of the bolt assembly quality is the key breakthrough point to find the manufacturing problem. Furthermore, the influence research of the bolt loosening under operating multiloading can provide an effective mean for bolt assembly inspection in advance.

The joint surface becomes the main source of nonlinearity and uncertainty of the rotating structure due to the discontinuity

(*) Corresponding author.
E-mail addresses:

C. Yue (ORCID: 0000-0002-2532-7195) yuecong234@163.com, X. Zheng (ORCID: 0000-0001-5965-4576) 1924411931@qq.com,
C. Wang cgwang@shmtu.edu, H. Liu liuhao8911@163.com, H. Chen chenhu@spic.com.cn

of mechanical contact and friction. Ibrahim A. Sever gave evidence of nonlinear vibration phenomena in aero engines from individual component to subsystems to the whole system [20]. It was shown that for bolt connection systems, it is very complex to capture the connection characteristics of each bolt. Subsequently, a large number of scholars analysed and modelled the nonlinear behaviour of bolt flange joint structures. They emphasized that the connection characteristics at the joint cannot be neglected in analysing the dynamic response of the system [6,7,8,11,18]. Luan et al. analysed the static mechanical properties of bolt flange joints for the piping structures, shows that the axial stiffness of bolt flange joints is different in tension and compression. In the analytical derivation, a special dynamic behaviour of coupled transverse and longitudinal vibrations was observed [10]. Wang et al. used an existing equivalent axial spring-bending beam model to describe the stiffness nonlinearity of a single bolt-flange joint section under tensile and compressive. Base on this, modelled the flexural stiffness of the entire bolt-flange joint, confirms that the stiffness loss of bolt flange joints is closely related to the load and assembly conditions [24]. Yu et al. used a new analytical model of bolt joints to describe nonlinearity under bending moments. It is shown that bolt joints produce stiffness loss and damping nonlinearity mainly in rotor systems [31]. Mir-Haidari et al. analysed the axial, normal, and radial stiffness of bolt flange joints with spigot. A novel and robust analytical formulation was proposed, and developed a general theoretical model to accurately characterize and capture the nonlinear dynamic response of aero-engine under various loading conditions [12]. All of the above studies have shown that the dynamic behaviour of bolt structures under different dynamic loads behaves in a complex manner. The essence is that the energy and damping dissipation at the bolt joints leads to nonlinear changes in the joint stiffness.

Numerous studies have shown that the nonlinear characteristics of the joint must be considered when analysing the dynamic response of a structure. The effect of bolt connections on the nonuniform distribution of the joint stiffness has also been verified by simulation models [1,3,25,28]. The time-varying stiffness at the joint interface during bolt missing was investigated using a three-dimensional nonlinear finite element model by Qin et al. The time-varying joint stiffness due

to bolt missing in rotors with drums and its effect on the steady-state response of the rotor were calculated. It provided a basis for studying the effect of bolt missing at the rotor joint interface on rotor dynamics [14,15]. Jie et al. discussed the effect of bending stiffness of aero-engine rotor joints under applied load. Taking a high-speed discontinuous rotor as an example, investigated the effect of joints on rotor dynamics by numerical and experimental research. [5]. Li et al. developed a bolt-connected disc rotor system to analyse the dynamic behaviour of bolt joints at different transition points with tangential and bending stiffnesses. The effect of the bending stiffness of the bolt joint disc on the system response was investigated [9]. Liu et al. used finite element nonlinear simulation and experimental method to analyse the dynamic characteristics of joints in an aero-engine rotor system. It showed that the stiffness and contact state of the joints vary with external loads and geometry. It affected the operation of the rotor system [18,21]. Nizametdinov et al. proposed an alternative method for analysing the dynamic characteristics of rotors. They used a combination of a general-purpose FEM composite and a specialized one, demonstrating that the value of the bending stiffness does not depend essentially on the geometry of the flange joint, but on the tightening force of the bolts, the axial force, the tensile joint, and the contact strain on the flange surface [13]. All the above studies show that the quality of bolt assembly directly affects the stiffness of the joint surface, causing an unavoidable effect on the response of the rotor dynamical system.

Bolt missing may cause a stiffness reduction [29]. A vibration-based method was proposed to monitor the structural health of bolt connection. This study was centered on detecting the reduction in stiffness due to the missing of bolt connection. Sun et al. developed a finite element model of an aero-engine high-pressure rotor system and studied the dynamic characteristics of the rotor system under different preload conditions. The study showed that the bolt preload decreases or loosens in the in-service condition, leading to loss or periodic changes in connection stiffness, which eventually affects the vibration response at the rotor connection positions. It can be used as a detection method for rotor bolt missing in rotating machinery [22]. Mohamed et al. proposed a frequency-based detection technique that uses the first transverse natural

frequency to quantify the tension and estimate the tightness of the bolts. Demonstrated the potential of frequency-based techniques for estimating bolt tightness [17]. Yue et al. used the MAE-XGBoost algorithm to predict the bolt dehiscence location by vibration response characteristics [32]. He et al. developed a vibration-based damage detection algorithm that uses structural natural frequency variations to detect whether exists bolt missing in rigid tubes with bolt flange joints [4,26,27]. Esmael et al. decomposed the vibration signal by EMD, and proposed an effective damage detection method, which bases on the energy index of the decomposed signal IMF to assess the structural health state. Established a vibration-based health monitoring strategy for detecting bolt missing in pipe bolt flange joints [2,16]. The change in stiffness directly affected the natural frequency of the system, and the above studies demonstrated the reliability of detecting bolt missing based on vibration signals.

In general, a large number of scholars have studied the nonlinear analysis of the bolt connection structure and the mechanism of stiffness loss due to the nonlinear connection characteristics of the joint, but most of them analysed the overall assembly quality of all bolts on the joint surface without considering the influence of bolts at different locations on the stiffness of the joint surface. This also led to the fact that the vibration signal detection method based on stiffness loss can only locate the joint surface with loose bolts, but cannot locate the specific bolt missing position on the joint surface.

In this paper, we analyse the quality detection of joint surface bolt assembly when the multistage disk-drum rotor is under great tension. In Section 2 analyses the connection stiffness of the single bolt equivalent action area when the whole multistage disk-drum rotor is under tension. A theoretical model of the equivalent stiffness of the joint surface is established to characterize the circumferential bolt position. Simulation results are also put forward to evaluate the circumferential distribution of the equivalent stiffness by the deviation state of bolt fastening at different directions. In Section 3, conducts a multi-exciting testing system to observe the vibration deviation of the single bolt missing at the key joint surface of multistage high-pressure rotor. Vibration resonance features under single bolt missing condition are obtained. In Section 4, the correlation of experimental data collected by each channel

sensor through the Spearman correlation coefficient. The connection between the eigenfrequency and the equivalent stiffness using the Intra-group Correlation Coefficient (ICC) is verified. The proposed theoretical model of identifying the circumferential direction of a single bolt loosening with equivalent stiffness is verified.

2. Material and methods

During the operation state of the multistage high pressure rotor system, the composite external forces including axial force and lateral vibration cause the partial deformation of each bolt at different circumferential directions. This section will analyse the stiffness characteristics of the flange sector acting on single bolt at the joint surface under integral tension. An equivalent stiffness model is established to introduce the stiffness loss caused by individual bolt missing at different directions. Numerical simulations show the influence of single bolt loosening at different circumferential directions.

2.1 Analysis of single bolt connection characteristics

The multistage disk-drum rotor system contains three main structural components: high-pressure pressurizer, combustion chamber and high-pressure turbine. As shown in Figure 1, the high-pressure simulated rotor test piece contains front shaft, three-stage pressurizer, turbine disk and rear shaft, with five joint surfaces. Each joint surface is symmetrically connected by M6 bolts, of which the first three joint surfaces contain 36 bolts, the fourth joint surface contains 24 bolts and the fifth joint surface contains 18 bolts, respectively. The fourth joint surface between the third stage compressor and turbine is the key structural joint position.

The schematic of the working area of a single bolt is shown in Figure 2. As shown in Figure 2.(a), the spigot friction can balance the external load and the spigot is in a state of adhesion when a smaller tensile load is applied. The spigot is slipped under the tensile load applied to the bolt is greater than spigot friction while the flange is deformed, which is shown in Figure 2.(b). When two flanges are tightened by bolt preload, the contact pressure exists only in a small area around the bolt. The angle α_c corresponds to the flange pressure area, which is related to the material and structure but independent of load [29]. α indicates the circumferential angle of the individual bolt action area corresponding to the joint surface.

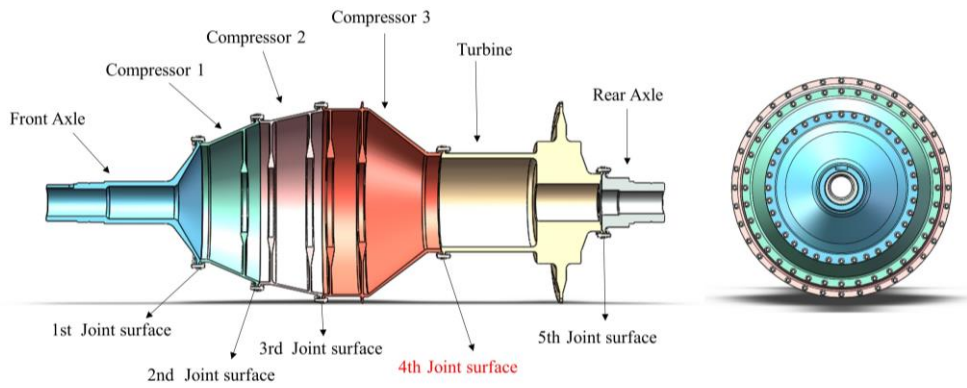


Fig. 1. structure cross-sectional view and left view of simulated rotor.

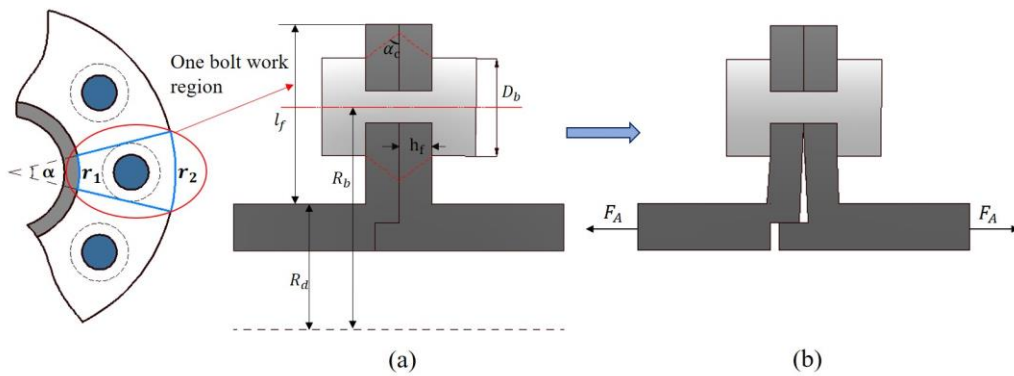


Fig. 2. Schematic diagram of the connection area of the flange bolt: (a) Bolts subjected to small loads. (b) Bolts subjected to large loads.

The angle α_c of the pressurized area of single bolt action flange is given in the earlier theoretical study [23] as the calculation formula:

$$\frac{1}{\tan \alpha_c} = 3 \sqrt{\left(\frac{D_b}{2h_f}\right)^3 + 0.61^3 + 0.53} - \frac{D_b}{2h_f} \quad (1)$$

α can be calculated by the following equation:

$$\alpha = \frac{D_b + 2h_f \tan \alpha_c}{R_b} \quad (2)$$

the bolt action area corresponds to the inner and outer flange

arc lengths can be calculated as follows:

$$\begin{cases} r_1 = \alpha \times R_d \\ r_2 = \alpha \times (R_d + l_f) \end{cases} \quad (3)$$

Figure 3 shows the flange beam model of single bolt action area in the flange joint surface, in which the bolt action is equated to the spring stiffness k_b . Point A is at the spigot, point B is at the bolt connection, and point C is at the flange separation, respectively. Thus, the internal relationship between the bolt connection and the bending stiffness of the entire flange position under axial tension can be obtained.

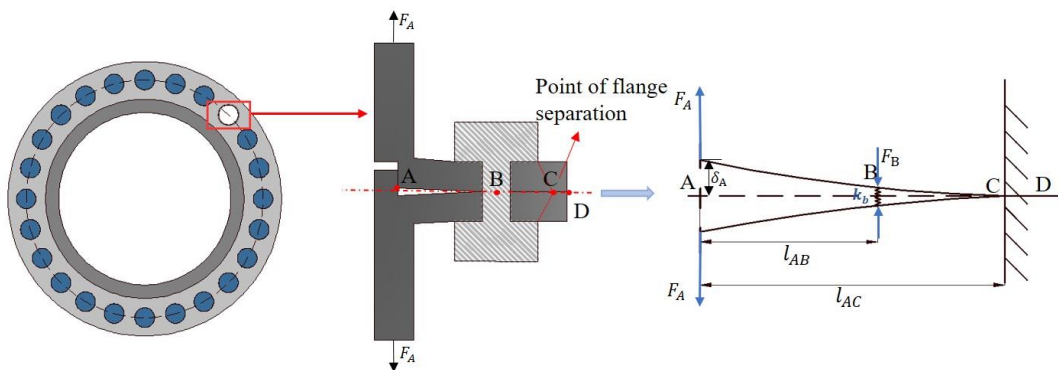


Fig. 3. Equivalent airfoil beam model for the area of single bolt action under axial tension.

Only the axial deformation of the flange is considered but without radial displacement, the moment balance equation can be expressed as:

$$F_A l_{AC} - F_B (l_{AC} - l_{AB}) = 0 \quad (4)$$

$$F_A + F_C - F_B = 0 \quad (5)$$

where F_A is the axial tension force, F_B is the bolt restraint force, F_C is the contact force, l_{AB} is the distance from the flange spigot to the center of the bolt connection, and l_{AC} is the distance from the flange spigot to the flange separation point. The approximate differential equation for the deflection curve is obtained from Equation (4):

$$\frac{F_A l_{AC}^2}{2EI_F} - \frac{F_B (l_{AC} - l_{AB})^2}{2EI_F} = 0 \quad (6)$$

where E is the Young's modulus of the flange and I_F is the equivalent moment of inertia of the bolt area. I_F can be calculated by the following equation [9].

$$I_F = \frac{h_f^3}{12} \left(\frac{16}{\frac{4}{3r_1+r_2} + \frac{4}{r_1+r_2} + \frac{36}{r_1+3r_2} + \frac{4}{r_2}} \right) \quad (7)$$

Meanwhile, the displacement and deflection of each position in the beam can be obtained. The displacement δ_B at point B can be expressed as:

$$\delta_B = \frac{F_A (l_{AC} - l_{AB})^2 [3l_{AC} - (l_{AC} - l_{AB})]}{6EI_F} - \frac{F_B (l_{AC} - l_{AB})^3}{3EI_F} \quad (8)$$

Deflection ω_B of point B is shown as Equation (9):

$$\omega_B = \frac{(F_B - F_0) h_f}{E_B d_B} \quad (9)$$

where F_0 indicates the bolt preload force, E_B indicates the Young's modulus of the bolt material, and d_B indicates the nominal diameter of the bolt.

$$\delta_B = \omega_B \quad (10)$$

the l_{AC} , F_B and F_C can be found by Equation (4), Equation (5) and Equation (10). the displacement δ_A of point A can be calculated as:

$$\delta_A = \frac{F_A l_{AC}^3}{3EI_F} - \frac{F_B (l_{AC} - l_{AB})^2 [3l_{AC} - (l_{AC} - l_{AB})]}{6EI_F} \quad (11)$$

the axial stiffness k_A of the flange in the area of a single bolt connection under axial tension is calculated as:

$$k_A = \frac{F_A}{2\delta_A} \quad (12)$$

2.2 Equivalent stiffness model of joint surface

There is a stretch deformation in the bolted joint surface because of the axial tensile caused by cycle operation. As a result, the bending moment is generated for the uneven distribution of axial force, in which the lower tensile deformation is large and the upper deformation is relatively small. Figure 4 illustrates the distribution of different circumferential positions at the bolted joint surface subjected to different degrees of axial tension. Therefore, bolts in different directions will suffer different degrees of connection stiffness loss.

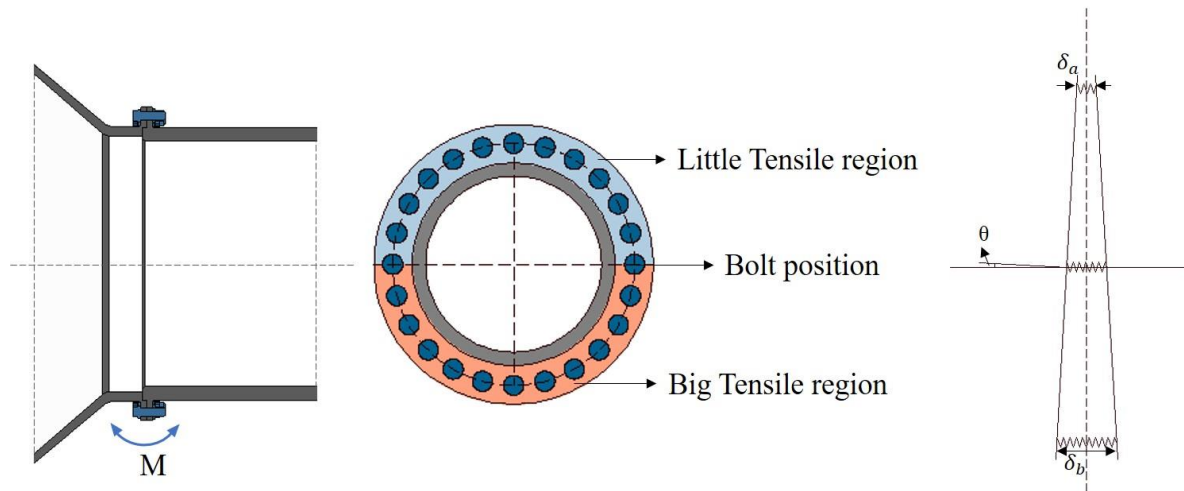


Fig. 4. Sketch of the joint surface's deformation under the action of bending moment.

The top bolt is marked with the initial serial number, and the remaining bolts are marked clockwise according to the intended

course. β_i indicates the circumferential angle of bolt i , as shown in Figure 5.

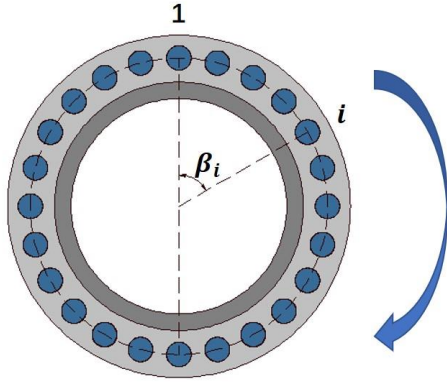


Fig. 5. Diagram of bolt numbering.

As the joint surface has n bolts for connection, β_i is expressed as:

$$\beta_i = 2\pi \frac{(i-1)}{n} \quad (13)$$

the bolt i shape variable δ_A can be calculated as:

$$\delta_i = \frac{\delta_a - \delta_b}{2R_d} (R_d + R_d \cos \beta_i) + \delta_b \quad (14)$$

the moment balance equation for the entire joint surface is as follows:

$$M = \sum_{i=1}^n F_i (1 + \cos \beta_i) R_d \quad (15)$$

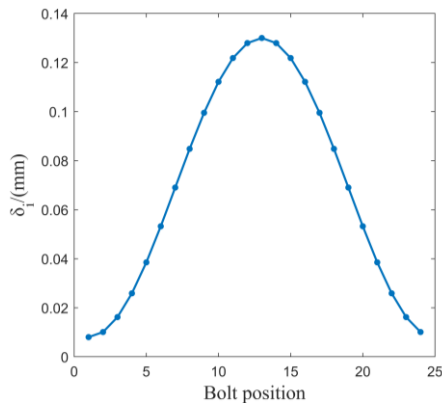
F_i indicates the magnitude of the axial tension on a single bolt, which can be expressed as:

$$F_i = k_A \delta_i \quad (16)$$

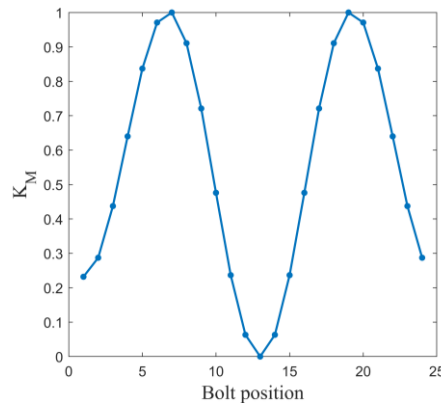
where k_A is calculated by Equation (11), Equation (12), and the bolt missing position of F_B is 0, causing k_A to decrease, the bolt connection area will have a loss of stiffness, θ is the bending angle, which can be expressed as:

$$\theta = \frac{\delta_a - \delta_b}{2R_d} \quad (17)$$

δ_a is the top tensile deformation and δ_b is the bottom tensile



a)



b)

Fig. 6. Simulation diagram of connection surface characteristics change by single bolt missing at different positions: (a) Flange deformation. (b) Normalized equivalent stiffness of joint surface.

deformation. In summary, the equivalent stiffness of the joint surface can be expressed as follows:

$$k_M = \frac{2MR_d}{\delta_a - \delta_b} = \frac{2R_b \sum_{i=1}^n k_A \delta_i (1 + \cos \beta_i) R_d}{\delta_a - \delta_b} \quad (18)$$

2.3 Numerical simulation analysis

The rotor is subjected to a large axial draw force so that each joint surface is under tension. For the multistage disk-drum rotor in Figure 1, the 4th joint surface is the key force surface. In this part, the equivalent radial stiffness distribution in the 4th joint surface is simulated numerically to study the effect of the single bolt missing at different directions.

The simulated rotor material and dimensional parameters are shown in Table 1.

Table 1. Material and dimensional parameters of simulated rotor system.

Parameters	Symbols	Unit	Value
Flange thickness	h_f	mm	4.5
Young's modulus of flange material	E	GPa	211
Drum radius	R_d	mm	100
Young's modulus of bolt material	E_B	GPa	115
Length from the bolt connection to the spigot	l_{AB}	mm	8.75
Bolt joint surface radius	R_b	mm	108.75
Bolt head diameter	D_b	mm	9.5
Nominal diameter of bolt	d_B	mm	6

The above parameters are algebraized into Equation (14) and Equation (18) for numerical simulation calculation. Considering the overall tension state of all bolts on the joint surface, the numerical simulation of variation tendency of the flange deformation δ_i by different bolt actions is shown in Figure 6.(a), and the normalized variation tendency for the equivalent stiffness at joint surface with single bolt missing at different positions is shown in Figure 6.(b).

The uneven force on the rotor under axial tension causes different deformation variables at different locations [14]. In addition, the simulated rotor placed transversely, the uneven axial tension makes the centre of gravity of the rotor shift slightly downward. Thus, the lower tensile deformation of the joint surface becomes large, and the upper deformation is relatively small. As shown in Figure 6, the flange deformation in the bolt connection area at different positions is distributed symmetrically on the left and right sides, and the downward deformation reaches the maximum. The equivalent radial stiffness of joint surface demonstrates the maximum value and horizontal symmetry by single bolt missing at different locations.

3. Experimental process and Data

In order to verify the validity of the proposed theoretical model, a single bolt loosening experiment under the compound

excitation of axial tension and lateral impact was carried out. This section introduces the experimental loading system, the experimental process and the extraction method of vibration characteristics, respectively.

The experimental equipment consists of a simulated rotor test bench, acceleration sensors, force hammer and digital extraction equipment, shown in Figure 7. Handheld force hammer is used to excite the system, and the acceleration sensors acquire vibration responses at different joint surfaces and key positions. The force hammer excitation position and sensor arrangement are shown in Figure 8. The digital acquisition instrument is used to acquire the vibration response signal of the rotor system. It is connected with DASP software to form a high-performance data acquisition and signal processing system with more than one hundred advanced technologies, and the resolution can reach 16kHz, which makes the experimental data reliable [32].

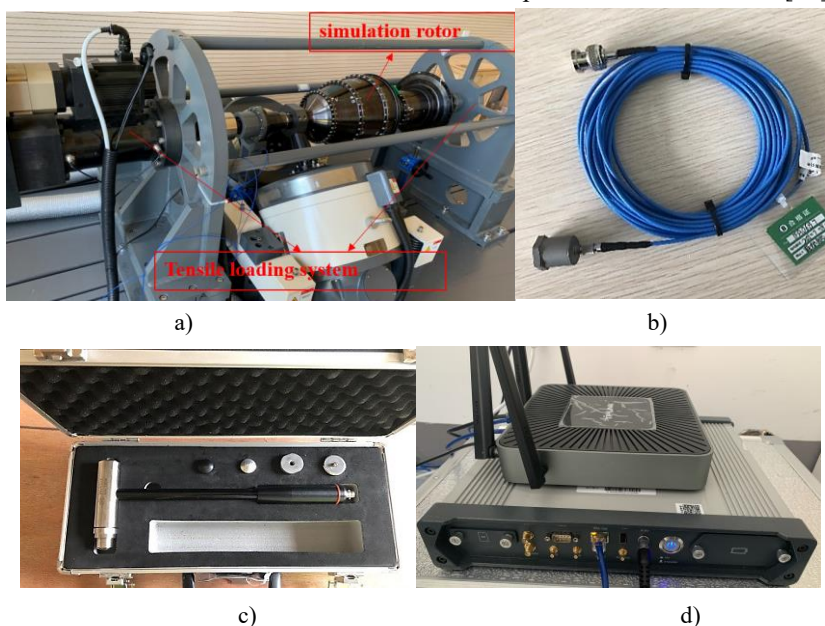


Fig. 7. Experimental equipment:(a)Rotor stiffness test bench. (b)Acceleration sensor. (c)Force hammer. (d)INV3062A model digital acquisition instrument.

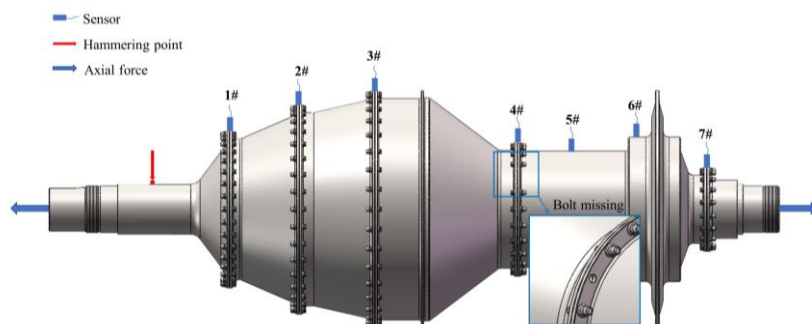


Fig. 8. Diagram of compound excitation and measuring point arrangement.

The fourth joint surface is the axial location of bolt loosening, and the bolt missing totally has 24 different circumferential positions. The single bolt missing vibration test is conducted under axial tension of 30kN and 25kN. The testing procedure is carried out by removing a single bolt in order while the other bolts are tightened with 8Nm. The experimental procedure is shown in Figure 9. The axial force variation is within $\pm 0.03\text{kN}$ to ensure that the vibration response variation is mainly from bolt loosening at different circumferential positions. The lateral impact provided by the hammering method also needs to be repeated three times to ensure stability and effectiveness. The sampling frequency of the acceleration sensor is 16kHz.

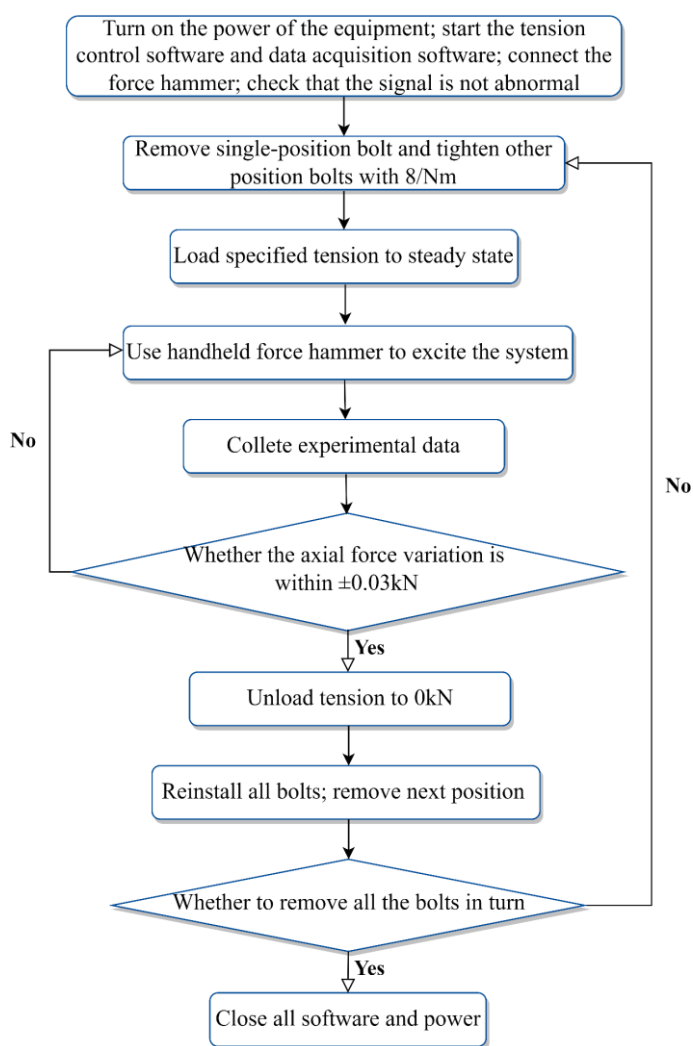


Fig. 9. Flow chart of the experiment process.

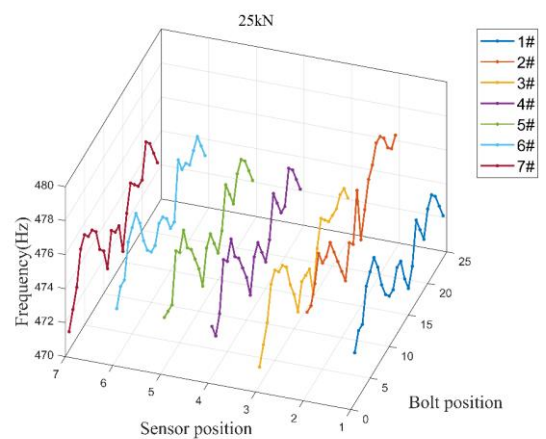
4. Results and Discussion

Due to the structural characteristics of the multistage rotor system and the loading mode oriented to compound load in operation, it is difficult to obtain the response difference of

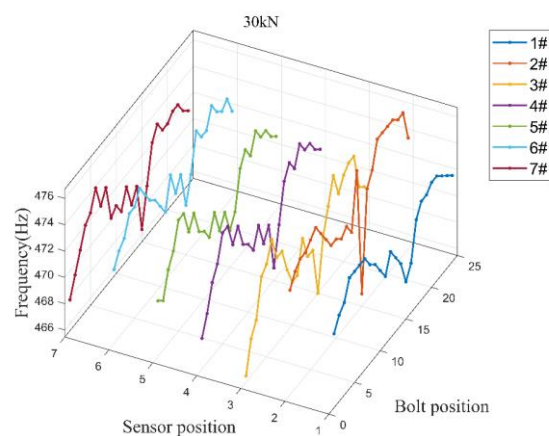
different measuring points directly. In this section, the correlation of vibration characteristics will be used to select the most appropriate measuring point position. The consistency of characteristic frequency and equivalent stiffness are verified.

4.1 Measuring point evaluation

The eigenfrequency of different vibration signals is collected by seven sensors along the axial direction. Figure 10 shows the 3D diagram of frequency characteristics of different measuring points under axial forces of 25kN and 30kN, respectively. The response variation trend of different measuring points is similar under the same working condition, and the eigenfrequency value under different coaxial forces has a certain distinction.



a)



b)

Fig. 10. Three-dimensional diagram of vibration characteristics under different conditions: (a) 25kN axial tension. (b) 30kN axial tension.

The axial arrangement of sensors makes different structural positions from the key joint surface, which may cause the

vibration response deviation by other joint surfaces. Correlation analysis can obtain the most relevant measuring points, which can indicate the most stability and reliability of the measured data to analyse the changes of response characteristics by single bolt loosening. In addition, Spearman correlation coefficient has a high adaptability when the data is non-continuous and abnormally distributed.

The heat map performance analysis of characteristic frequency correlation of each sensor is shown in Figure 11. The result shows that the sensor 4# and the sensor 5# have the strongest correlation coefficient, which reach 95.68% and 99.32% under the axial tension force of 25kN and 30kN, respectively. It seems that the transmission path of multistage drum structure affects the vibration response of connection deviation.

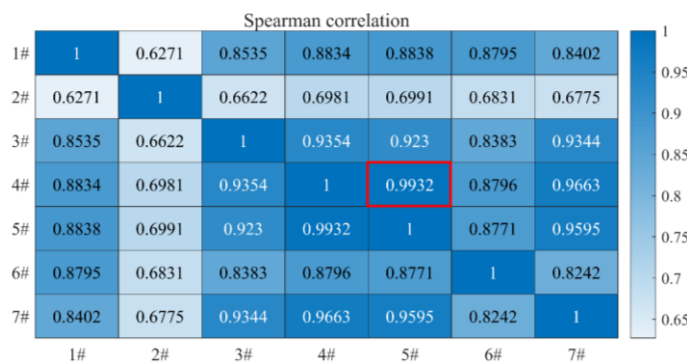
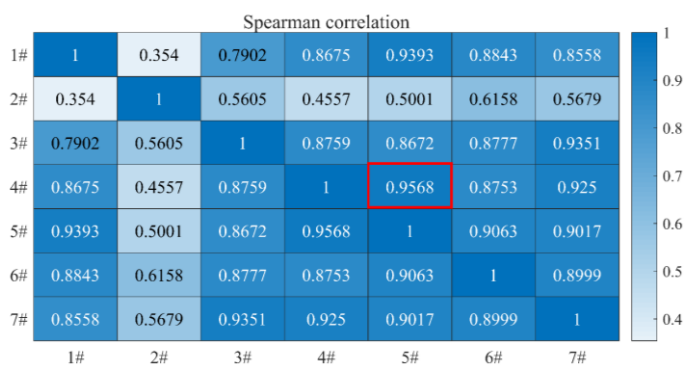


Fig. 10. Correlation analysis of each sensor under different tension forces: (a) 25kN axial tensile force. (b) 30kN axial tensile force.

Figure 12 shows the frequency response curves of different bolt loosening conditions by the same sensor, in which the vibration response is in the range of 0-1000Hz under the same loading condition. In general, the response curves are less differentiated. However, relatively obvious differences can be found in the resonance frequency peak of 470Hz from the rotor

system. As a result, the peak value near 470Hz is extracted as the characteristic frequency because of not only the resonant frequency but also the obvious differences of different bolt loosening.

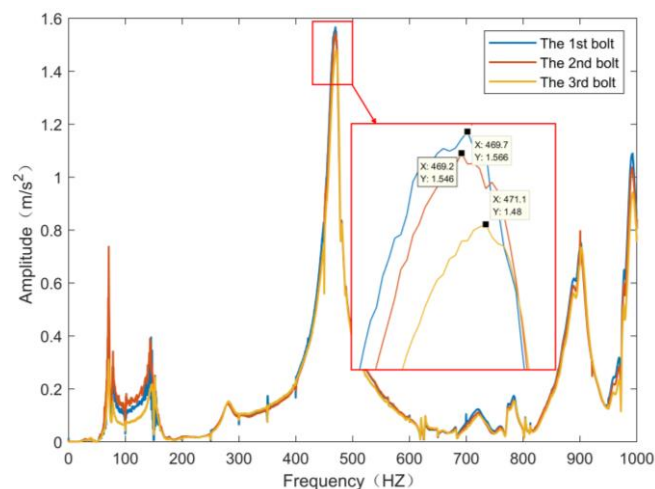
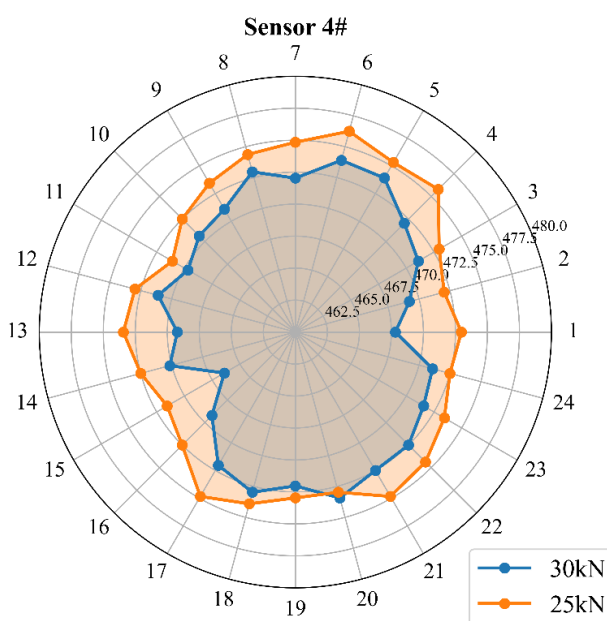


Fig. 11. Frequency response of one bolt missing at different circumferential positions under 30kN of Sensor 4#.

The eigenfrequency of sensor 4# and sensor 5# under two tension forces are shown in Figure 13. It can be observed that the eigenfrequency is greater when the joint surface maintains stable connection performance. Meanwhile, although the validity of experimental results is improved by controlling the fluctuation range of axial force and repeated impact force, the distribution of frequency peak still fluctuates at some bolt loosen positions.



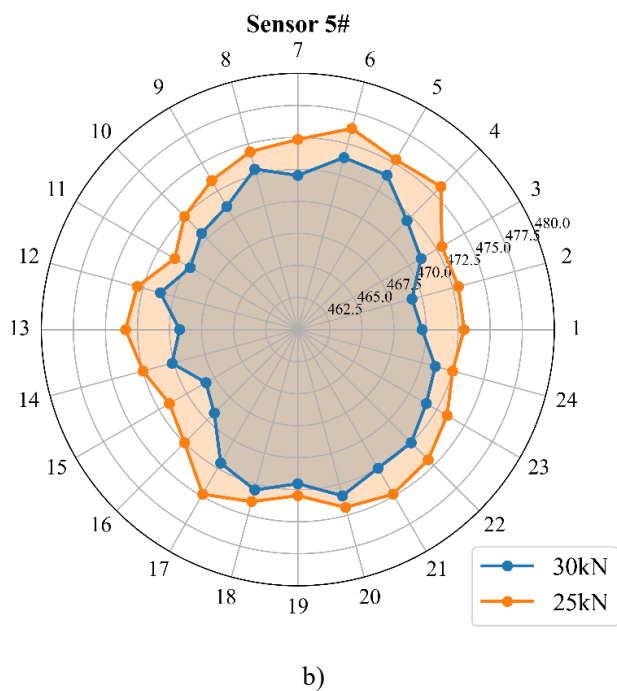


Fig. 12. Eigenfrequency of different sensors under axial tension forces: (a) Sensor 4#. (b) Sensor 5#.

4.2 Equivalent stiffness model verification

In order to locate the loose circumferential direction of the bolt, the eigenfrequencies of sensor 4# and sensor 5# under 30kN axial tension force loading are associated with the equivalent stiffness in the calculation model. Figure 14 illustrates the normalized eigenfrequency and equivalent stiffness in the same condition of 30kN axial force and bolt loosening. It can observe that the eigenfrequencies at the bolt positions numbered 12-14 have a small tendency to become larger, which may be related to the structural stiffness loss weakened by friction and viscous damping. The ICC is used to evaluate the consistency of these two data groups, and Table 2 demonstrates the test results. The correlation coefficient reached 0.889, which indicates that there is a strong consistency between equivalent stiffness and characteristic frequency. (ICC greater than 0.75 indicates strong consistency of the data.)

From above analysis, the distribution of equivalent bending stiffness of bolt tension connection has a strong consistency with the eigenfrequency of system vibration, and the stiffness loss by bolt loosening can be illustrated by detecting the eigenfrequency. The equivalent stiffness loss by bolt missing at different locations has circumferential symmetry, and the corresponding eigenfrequency also varies accordingly. In the circumferential tensile state, the possibility that the specific

location of bolt loosening deviation can be quickly analysed and located by the characteristic frequency of a specific measuring point is verified by the equivalent model and experiment.

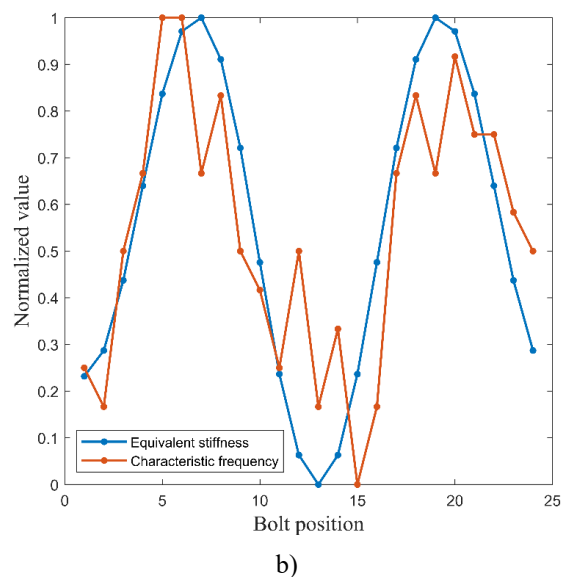
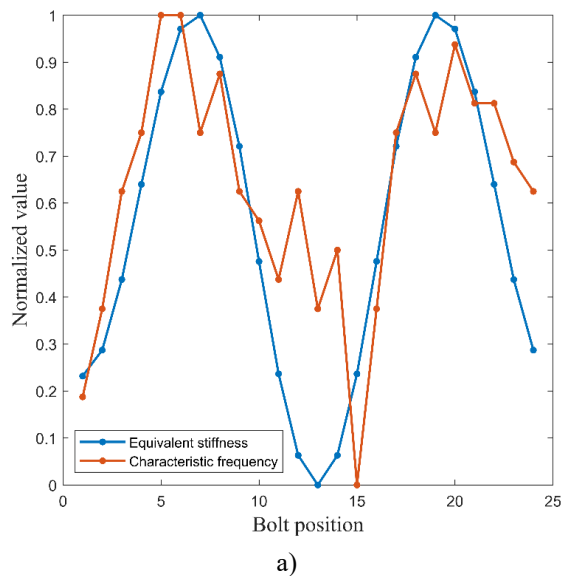


Fig. 13. Comparison diagram of Normalized equivalent stiffness and eigenfrequency: (a) Sensor 4#. (b) Sensor 5#.

Table 2. ICC analysis between equivalent stiffness and characteristic frequency.

	ICC	95% confidence interval	P value
ICC(1,k)	0.889	0.747-0.952	0.000*** ¹

¹*** represents 1% significance level

From above analysis, the distribution of equivalent bending stiffness of bolt tension connection has a strong consistency with the eigenfrequency of system vibration, and the stiffness loss by bolt loosening can be illustrated by detecting the eigenfrequency. The equivalent stiffness loss by bolt missing at

different locations has circumferential symmetry, and the corresponding eigenfrequency also varies accordingly. In the circumferential tensile state, the possibility that the specific location of bolt loosening deviation can be quickly analysed and located by the characteristic frequency of a specific measuring point is verified by the equivalent model and experiment.

In summary, the equivalent bending stiffness model can be used to determine the influence of bolt deviation degree on the overall bending stiffness of joint surface. Vibration and axial loading experiment of multistage rotor with bolt missing can be used in engineering to inspect the quality of bolt assembly, and the influence of service performance on bolt joint surface effectively.

5. Conclusions

In this paper, based on the bolting characteristics of a multistage disk-drum rotor system, an equivalent bending stiffness model for the stiffness loss caused by bolt connection deviation under axial tension force was established. The vibration experiment of single bolt missing by axial tension force and impact load was carried out to obtain the dynamic response. The experimental results were used to analyse the correspondence between the equivalent bending stiffness of joint surface and the vibration characteristics for single bolt

missing. The effectiveness of the proposed method was verified. The conclusions are as follows:

1. The equivalent bending stiffness model single bolt missing takes the axial tensile load into account. This model is used to detect the relationship between connection deviation of bolt preload and the Joint stiffness of joint surface;
2. The multi-axis excitation experiment of single bolt missing controls the axial tension up to 25kN and 30kN within ± 0.03 kN fluctuation. The effective resonant frequency and vibration characteristics are obtained by controlling the accuracy and stability of the experimental load;
3. ICC of normalized eigenfrequencies and equivalent stiffness reaches 88.9%, which indicates that the equivalent stiffness and the eigenfrequency have a high consistency with the influence trend of bolt missing at different circumferential positions. It is verified that the established equivalent model can reflect the main vibration characteristics with the bolt loosening under axial tension.

The current study was conducted to analyse the stiffness loss caused by single bolt loosening at the critical joint surface when the aero-engine rotor is in operation. Research and verification of the joint surface stiffness loss caused by different degrees of bolt assembly deviations under different axial forces will be further considered later.

Acknowledgements

The authors would like to thank Huashan Chi and Jianyu Fan for their help in experiment. The authors gratefully acknowledge the financial support for this project from the National Natural Science Foundation of China Youth Fund, grant number 5220511.

References

1. Beaudoin, M.-A.; Behdinin, K. Analytical lump model for the nonlinear dynamic response of bolted flanges in aero-engine casings. *Mechanical Systems and Signal Processing* 2019; 115: 14-28, <https://doi.org/10.1016/j.ymsp.2018.05.056>
2. Briand, J.; Esmaeel, R.A.; Taheri, F. Computational simulation and experimental verification of a new vibration-based structural health monitoring approach using piezoelectric sensors. *Structural Health Monitoring-an International Journal* 2012, <https://doi.org/10.1177/1475921711414239>
3. Du, D.; Sun, W.; Ma, H.; Yan, X.; Liu, X. Vibration characteristics analysis for rotating bolted joined cylindrical shells considering the discontinuous variable-stiffness connection. *Thin-Walled Structures* 2022; 177, <https://doi.org/10.1016/j.tws.2022.109422>
4. He, K.; Zhu, W.D. Detecting Loosening of Bolted Connections in a Pipeline Using Changes in Natural Frequencies. *Journal of Vibration and Acoustics* 2014; 136, <https://doi.org/10.1115/1.4026973>
5. Hong, J.; Chen, X.; Wang, Y.; Ma, Y. Optimization of dynamics of non-continuous rotor based on model of rotor stiffness. *Mechanical Systems and Signal Processing* 2019; 131: 166-182, <https://doi.org/10.1016/j.ymsp.2019.05.030>
6. Kim, Y.J.; Madugula, M.K.S. Behavior of bolted circular flange connections subject to tensile loading. *International Journal of Steel Structures* 2010, <https://doi.org/10.1007/BF03249512>
7. Li, G.; Nie, Z.; Zeng, Y.; Pan, J.; Guan, Z. New Simplified Dynamic Modeling Method of Bolted Flange Joints of Launch Vehicle. *Journal*

- of Vibration and Acoustics 2020; 142, <https://doi.org/10.1115/1.4045919>
8. Li, T.; Yang, D.; Zhao, B.; Sun, Q.; Huo, J.; Sun, W. Measured and investigated nonlinear dynamics parameters on bolted flange joints of combined rotor. *Journal of Mechanical Science and Technology* 2021; 35: 1841-1850, <https://doi.org/10.1007/s12206-021-0404-8>
 9. Li, Y.; Luo, Z.; Liu, J.; Ma, H.; Yang, D. Dynamic modeling and stability analysis of a rotor-bearing system with bolted-disk joint. *Mechanical Systems and Signal Processing* 2021; 158, <https://doi.org/10.1016/j.ymssp.2021.107778>
 10. Luan, Y.; Guan, Z.-Q.; Cheng, G.-D.; Liu, S. A simplified nonlinear dynamic model for the analysis of pipe structures with bolted flange joints. *Journal of Sound and Vibration* 2012; 331: 325-344, <https://doi.org/10.1016/j.jsv.2011.09.002>
 11. Meisami, F.; Moavenian, M.; Afsharfard, A. Nonlinear behavior of single bolted flange joints: A novel analytical model. *Engineering Structures* 2018; 173: 908-917, <https://doi.org/10.1016/j.engstruct.2018.07.035>
 12. Mir-Haidari, S.-E.; Behdinin, K. Nonlinear effects of bolted flange connections in aeroengine casing assemblies. *Mechanical Systems and Signal Processing* 2022; 166, <https://doi.org/10.1016/j.ymssp.2021.108433>
 13. Nizametdinov, F.R.; Romashin, Y.S.; Berne, A.L.; Leontyev, M.K. Investigation of Bending Stiffness of Gas Turbine Engine Rotor Flanged Connection. *Journal of Mechanics* 2020; 36: 729-736, <https://doi.org/10.1017/jmech.2020.14>
 14. Qin, Z.; Han, Q.; Chu, F. Bolt loosening at rotating joint interface and its influence on rotor dynamics. *Engineering Failure Analysis* 2016; 59: 456-466, <https://doi.org/10.1016/j.engfailanal.2015.11.002>
 15. Qin, Z.Y.; Han, Q.K.; Chu, F.L. Analytical model of bolted disk-drum joints and its application to dynamic analysis of jointed rotor. *Proceedings of the Institution of Mechanical Engineers, Part C: Journal of Mechanical Engineering Science* 2013; 228: 646-663, <https://doi.org/10.1177/0954406213489084>
 16. Razi, P.; Esmaeel, R.A.; Taheri, F. Improvement of a vibration-based damage detection approach for health monitoring of bolted flange joints in pipelines. *Structural Health Monitoring* 2013; 12: 207-224, <https://doi.org/10.1177/1475921713479641>
 17. Sah, S.M.; Thomsen, J.J.; Brøns, M.; Fidlin, A.; Tcherniak, D. Estimating bolt tightness using transverse natural frequencies. *Journal of Sound and Vibration* 2018; 431: 137-149, <https://doi.org/10.1016/j.jsv.2018.05.040>
 18. Schwingshackl, C.W.; Di Maio, D.; Sever, I.; Green, J.S. Modeling and Validation of the Nonlinear Dynamic Behavior of Bolted Flange Joints. *Journal of Engineering for Gas Turbines and Power* 2013; 135, <https://doi.org/10.1115/1.4025076>
 19. Schwingshackl, C.W.; Petrov, E.P. Modeling of Flange Joints for the Nonlinear Dynamic Analysis of Gas Turbine Engine Casings. *Journal of Engineering for Gas Turbines and Power* 2012; 134, <https://doi.org/10.1115/1.4007342>
 20. Sever, I.A. Nonlinear Vibration Phenomena in Aero-Engine Measurements. In *Dynamics of Coupled Structures, Volume 4; Conference Proceedings of the Society for Experimental Mechanics Series*; 2016; pp. 241-252. https://doi.org/10.1007/978-3-319-29763-7_23
 21. Shuguo, L.; Yanhong, M.; Dayi, Z.; Jie, H. Studies on dynamic characteristics of the joint in the aero-engine rotor system. *Mechanical Systems and Signal Processing* 2012; 29: 120-136, <https://doi.org/10.1016/j.ymssp.2011.12.001>
 22. Sun, W.; Li, T.; Yang, D.; Sun, Q.; Huo, J. Dynamic investigation of aeroengine high pressure rotor system considering assembly characteristics of bolted joints. *Engineering Failure Analysis* 2020; 112, <https://doi.org/10.1016/j.engfailanal.2020.104510>
 23. Thompson, J.C.; Sze, Y.; Strevel, D.G.; Jofriet, J.C. The Interface Boundary Conditions for Bolted Flanged Connections. *Journal of Pressure Vessel Technology* 1976; 98: 277, <https://doi.org/10.1115/1.3454412>
 24. Wang, C.; Zhang, D.; Zhu, X.; Jie, H. Study on the Stiffness Loss and the Dynamic Influence on Rotor System of the Bolted Flange Joint. *American Society of Mechanical Engineers* 2014, <https://doi.org/10.1115/GT2014-26191>
 25. Wang, Y.Q.; Zong, L.; Shi, Y.J. Bending behavior and design model of bolted flange-plate connection. *Journal of Constructional Steel Research* 2013; 84: 1-16, <https://doi.org/10.1016/j.jcsr.2013.01.012>
 26. Wong, C.N.; Zhu, W.D.; Xu, G.Y. On an iterative general-order perturbation method for multiple structural damage detection. *Journal of Sound and Vibration* 2004; 273: 363-386, [https://doi.org/10.1016/s0022-460x\(03\)00543-1](https://doi.org/10.1016/s0022-460x(03)00543-1)
 27. Xu, G.Y.; Zhu, W.; Emory, B.H. Experimental and Numerical Investigation of Structural Damage Detection Using Changes in Natural Frequencies. *Journal of Vibration and Acoustics* 2007, <https://doi.org/10.1115/1.2731409>
 28. Yao, X.; Wang, J.; Zhai, X. Research and application of improved thin-layer element method of aero-engine bolted joints. *Proceedings of the Institution of Mechanical Engineers, Part G: Journal of Aerospace Engineering* 2016; 231: 823-839, <https://doi.org/10.1177/0954410016643978>

29. Yao, X.; Wang, J. Effects of load and structure parameters of aero-engine bolted joints on joint stiffness. *Tuijin Jishu/Journal of Propulsion Technology*. 2017; 3,622: 424–433, <https://doi.org/10.13675/j.cnki.tjjs.2017.02.022>
30. You, J.M.; Hong, Y.C.; Jeon, S.H.; Huh, J.; Ahn, J.-H. Behavior of bolt-connected steel plate girder attributable to bolt loosening failure in the lower flange. *Engineering Failure Analysis* 2020; 107, <https://doi.org/10.1016/j.engfailanal.2019.104208>
31. Yu, P.; Li, L.; Chen, G.; Yang, M. Dynamic modelling and vibration characteristics analysis for the bolted joint with spigot in the rotor system. *Applied Mathematical Modelling* 2021; 94: 306-331, <https://doi.org/10.1016/j.apm.2021.01.028>
32. Yue, C.; Chi, H.; Fan, J.; Zheng, X.; Zhang, Z. Prediction of bolt missing fault for multistage rotor by experimental test and analysis. *The International Journal of Advanced Manufacturing Technology* 2023; 124: 4551-4562, <https://doi.org/10.1007/s00170-022-10356-3>